metals

MDPI

Communication

Effects of Thermal Aging on the Low Cycle Fatigue Behaviors of Cast Duplex Stainless Steels

Shilei Li [1,*], Yanli Wang [1] and Xitao Wang [2,3,*]

[1] State Key Laboratory for Advanced Metals and Materials, University of Science and Technology Beijing, Beijing 100083, China; wangyl@ustb.edu.cn

[2] Collaborative Innovation Center of Steel Technology, University of Science and Technology Beijing, Beijing 100083, China

[3] Shandong Provincial Key Laboratory for High Strength Lightweight Metallic Materials, Advanced Materials Institute, Qilu University of Technology, Shandong Academy of Science, Jinan 250353, China

* Correspondence: lishilei@ustb.edu.cn (S.L.); xtwang@ustb.edu.cn (X.W.); Tel.: +86-135-5272-7287 (S.L.); +86-139-1029-7623 (X.W.)

Received: 6 March 2019; Accepted: 22 March 2019; Published: 25 March 2019

Abstract: The low cycle fatigue (LCF) behaviors of cast duplex stainless steel (CDSS) thermally aged at different times were investigated under different strain amplitudes. The effects of thermal aging on the LCF lives of CDSS are closely related to the strain amplitude. At a low strain amplitude, the fatigue life of the material increases significantly after thermal aging, while the LCF life decreases with an increasing aging time at a high strain amplitude. After thermal aging at 400 °C for 10,000 h, the fatigue fracture morphologies of CDSS change from fatigue fringes to mixture features including fatigue fringes in austenite and cleavage cracks in ferrite. Severe plastic deformation in ferrite of the aged CDSS under a high strain amplitude causes the cleavage cracking of ferrite. The premature failure of ferrite accelerates the propagation of fatigue crack and shortens the fatigue life at a high strain amplitude.

Keywords: cast duplex stainless steels; thermal aging; fatigue

1. Introduction

Cast duplex stainless steels (CDSSs) have excellent performances on mechanical properties, corrosion resistance, and weldability because of their dual phase microstructure of austenite and ferrite [1–3]. CDSS components are known to be sensitive to embrittlement after long-term thermal aging at moderate temperatures [4–7]. Spinodal decomposition in ferrite of CDSS during thermal aging is widely regarded as the primary mechanism of embrittlement [8–12]. Earlier studies indicated that long-term thermal aging caused the degradation in mechanical properties, such as impact properties, hardness, and tensile properties [13–16]. It was found that the impact toughness of CDSS decreased with an increasing aging time and the ductile-to-brittle transition in the impact fracture occurred after long-term thermal aging [17]. The ferrite hardness increased with the aging time, but the hardness in austenite had no obvious change [18,19]. The tensile strength of CDSS was not strongly affected by thermal aging, but the plasticity had a significant decrease after long-term aging [20].

Chen et al. reported that the low cycle fatigue (LCF) life of CDSS was prolonged at all strain amplitudes as thermal aging duration increases up to 6000 h at 400 °C [21]. However, Llanes et al. considered that the effects of thermal aging on the cyclic deformation mechanisms of a duplex stainless steel were strongly related to the plastic strain amplitude [22]. The investigation of fatigue crack initiation behavior in SAF 2205 DSS (aged at 475 °C for 100 h) indicated that the intersection of slip markings and phase boundaries were the triggering points of fatigue crack initiation [23]. Marrow et al. considered that the fatigue crack propagation in a thermally aged duplex is associated with the cleavage of the age-hardened ferrite phase, initiated by deformation twinning [24]. The aim of this study is to clarify the effect of strain amplitude on the LCF behaviors and the damage mechanism of the aged CDSS under cyclic deformation. The CDSS specimens thermally aged at different times were adopted. The fatigue tests under different strain amplitudes were performed. The fatigue fracture morphologies and the deformed microstructures were also observed.

2. Materials and Methods

The chemical composition of the studied CDSS was analyzed in accordance with the standard of ASTM E353-14 for chemical analysis methods and the result is listed in Table 1. After centrifugal casting, the CDSS was solution treated at 1080 °C for 8 h and then quenched in water. The studied steel has the duplex phase microstructure: Ferrite (15%) + austenite (85%), as shown in Figure 1a. The specimen was mechanically polished and etched using a solution (5 g $FeCl_3$ + 100 mL HCl + 100 mL + CH_3OH + 100 mL H_2O) to distinguish ferrite from the austenite matrix. The CDSS specimens were thermally aged at 400 °C for 3000, 7000, and 10,000 h in order to investigate the influence of thermal aging on their LCF properties.

Table 1. Chemical composition of the studied steel.

Element	Cr	Ni	Mn	Si	Mo	C	N	S	P	Fe
wt.%	20.45	10.2	1.02	1.15	0.2	0.031	0.091	0.0032	0.026	balance

The LCF tests were conducted using an MTS 809 axial torsion materials testing system (MTS, Eden Prairie, MN, USA) at room temperature in accordance with the standard of ASTM E606/E606M-12. The total strain control was used a triangular waveform with a strain ratio of R = −1 under different total strain ranges of 0.2%, 0.3%, 0.4%, 0.5%, and 0.6%. The cylindrical specimens with thread-button head were cut form the unaged and aged (at 400 °C for 3000, 7000, and 10,000 h) CDSS with a gauge length of 30 mm and diameter of 6.3 mm, as shown in Figure 1b. The engineering stress-strain curves of the unaged and aged (400 °C, 10,000 h) CDSS were shown in Figure 1c. The LCF tests were continued until the specimen fractured, whereby the life criterion was defined as the 30% drop of the tensile stress. The fracture surface morphologies of the fatigue specimens were observed in a scanning electron microscopy (SEM, ZEISS Supra 55, Oberkochen, Germany). The deformed microstructure of the fatigued specimen was observed by a transition electron microscopy (TEM, FEI Tecnai F30, Eindhoven, The Netherlands) operated at 300 kV.

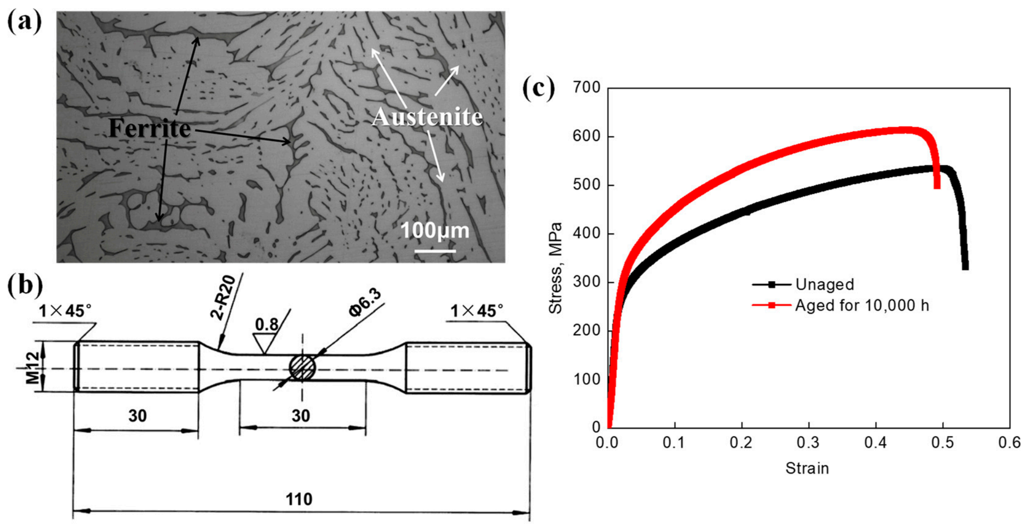

Figure 1. (**a**) Microstructure of the studied steel. (**b**) Geometry of the fatigue specimen (unit: mm). (**c**) Engineering stress-strain curves of the unaged and aged (400 °C, 10,000 h) CDSS.

3. Results and Discussions

The cycle stress response curves of the unaged and aged CDSS are shown in Figure 2. The variation of the stress amplitude of the material under cyclic loading can be divided into four stages: (1) The cyclic hardening stage, where the stress amplitude rapidly rises to the maximum stress amplitude in the first few cycles; (2) the slow cyclic softening stage, where the material begins to soften once the maximum stress amplitude was reached; (3) the cyclic saturation stage, where the stress amplitudes stay unchanged with cycles; (4) the rapid softening stage, where the material softens and eventually fractures. The cyclic stress response characteristics of the unaged and aged materials were closely related to the strain amplitude. Under low strain amplitude, cyclic softening occurred after initial short cyclic hardening, followed by the cyclic saturation stage, which accounted for more than half of the total life. While the cyclic saturation stage was much shorter under high strain amplitude, the cycle softening stage accounted for more than half of the total life. Compared with the unaged materials, the degree of cyclic hardening and softening of the aged materials was more pronounced, and the proportion of the cycle hardening stage in the total life was higher. The values of both the maximum and saturated stress amplitudes of CDSS tested at high strain amplitude increased after thermal aging, while they had the opposite trend at low strain amplitude. The LCF lives of both the unaged and aged specimens gradually decreased with increasing strain amplitude from 0.2 to 0.6%. The effect of thermal aging on fatigue life was closely related to the strain amplitude. At low strain amplitudes, the fatigue life of the material increases significantly after thermal aging. Under the strain amplitude of 0.2%, the CDSS thermal aged at 400 °C for 10,000 h was still not broken after 80,000 cycles. At high strain amplitudes, the LCF life of the material decreased after thermal aging. Under the strain amplitude of 0.6%, the cyclic life of the aged CDSS reduced by 40% compared with the unaged CDSS.

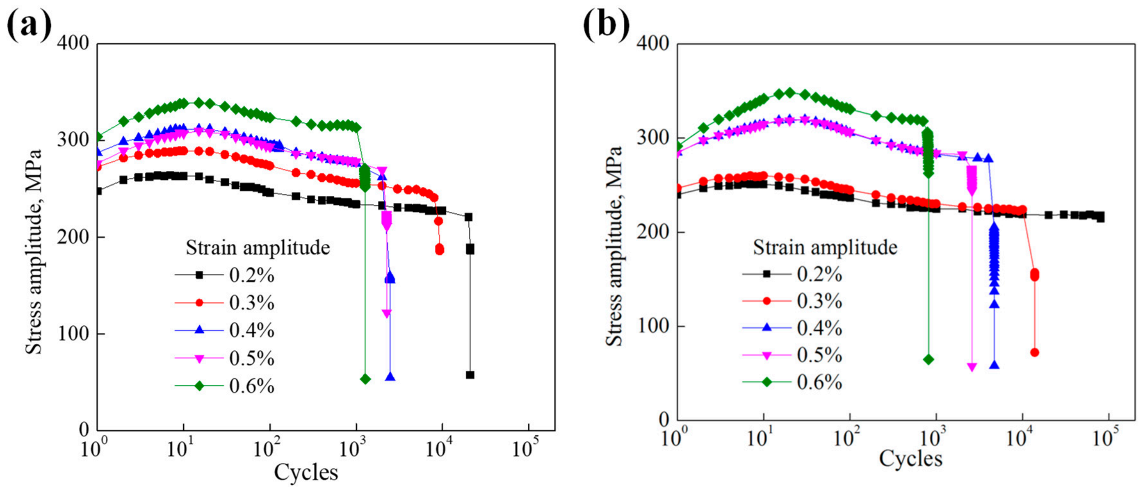

Figure 2. Cyclic stress response curves of the CDSS. (**a**) Unaged, (**b**) Thermal aged at 400 °C for 10,000 h.

The Coffin–Manson model was used to fit the LCF experimental data at different aging states and Table 2 lists all the parameters. In accordance with the determined parameters, Figure 3a shows the variation of fatigue life with strain amplitude for the CDSS unaged and aged at 400 °C for 3000, 7000, and 10,000 h. For the same thermal aging state, the LCF life of the material decreased linearly with increasing strain amplitude. The stable hysteresis loops under 0.2 and 0.6% strain amplitudes (at half of the fatigue life) of specimens with different aging states are shown in Figure 3b. Under low strain amplitude, thermal aging has no significant effect on the stable hysteresis loop of both the unaged and aged CDSS. The area of the stable stress-strain hysteresis loop of the aged CDSS under high strain amplitude was larger than that of the unaged material. With the increase of aging time, the increasing energy per cycle under high strain amplitude accelerated the damage of material, resulting in the decrease of fatigue life.

Table 2. Coffin–Manson parameters of materials at different aging states.

Parameters	ε'_f	c
Unaged	0.400	−0.606
Aged for 3000 h	0.359	−0.603
Aged for 7000 h	0.262	−0.569
Aged for 10,000 h	0.100	−0.457

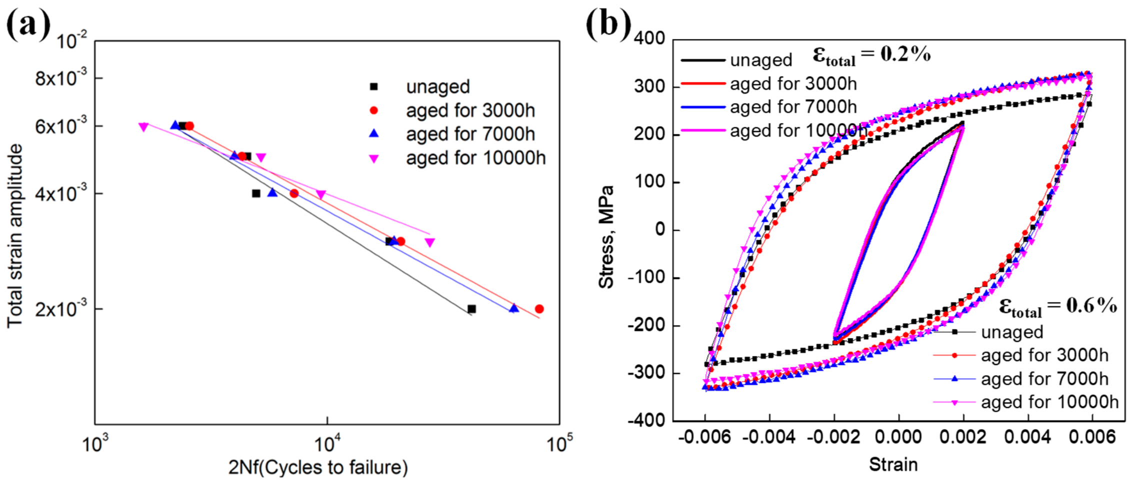

Figure 3. (**a**) Variation of fatigue life of the unaged and aged CDSS with strain amplitude. (**b**) Stable hysteresis loops under 0.2 and 0.6% strain amplitude of specimens with different aging states.

The fatigue fracture surfaces under all conditions in the present study include three regions: The crack initiation region, the fatigue crack growth region (with beach markings), and the rapid rupture region. Under low strain amplitude, only one crack origin forms on the fracture surface of the unaged and aged CDSS samples. While several sites of crack origin were observed on the surfaces of the unaged and aged samples under high strain amplitude. Dimple is the main feature of the rapid rupture region for all samples and some brittle fracture features were observed only on the surface of the aged sample under high strain amplitude. The difference in the fatigue fracture morphology caused by thermal aging and strain amplitude mainly occurred in the crack growth region. The morphologies of fatigue crack growth regions in the unaged and aged CDSS under 0.2 and 0.6% strain amplitudes are shown in Figure 4. Both the ferritic and austenitic phases displayed fatigue fringes on the fatigue fracture surfaces of the fatigue crack growth regions in unaged CDSS under a strain amplitude of 0.2%, and the two phases could not be distinguished from each other. When the strain amplitude increased to 0.6%, the fatigue fringe spacing of the unaged CDSS significantly broadens. The fatigue fracture morphologies of CDSS after thermal aging for 10,000 h were significantly different from the unaged. The ferritic and austenitic phases on the fatigue fracture surface display different characteristics, and the fatigue fringes mainly appear in austenite. The fatigue fringes in the austenite of the aged CDSS under 0.6% strain amplitude were denser than those in the unaged material. Brittle cleavage characteristics and micro-cracks in ferrite were observed on the fracture surface of the aged CDSS under 0.6% strain amplitude. The micro-cracks in ferrite of the aged CDSS led to a significant decrease in fatigue life.

In order to investigate the deformation mechanism in the unaged and aged CDSS during cyclic loading under different strain amplitudes, the deformed microstructures were observed in TEM. A TEM sample was cut from the fatigue fracture surface of the unaged and aged CDSS under a strain amplitude of 0.3% and 0.6%. Our previous studies have shown that the mechanical property degradation of CDSS induced by thermal aging is mainly caused by the hardening and embrittlement in ferrite [17,18]. Thus, the observation of the deformed structures of the fatigued samples is focused on the dislocation structures in ferrite. Figure 5a–d displays the TEM images of ferrite in the fatigued specimen of the unaged and aged under strain amplitude of 0.3% and 0.6%.

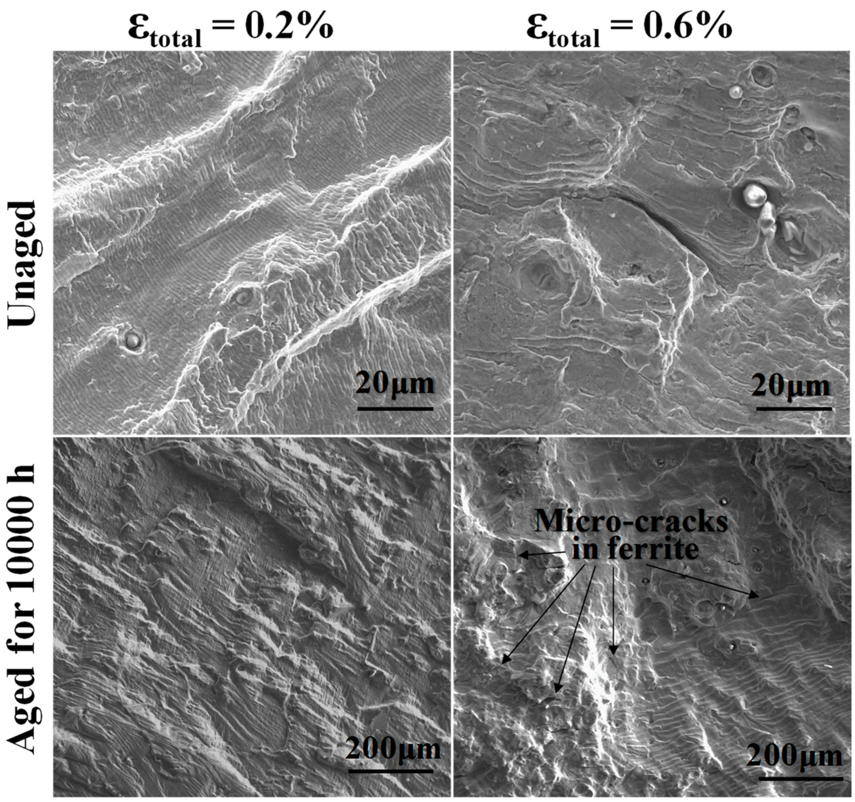

Figure 4. The morphologies of the fatigue crack growth regions in the unaged and aged CDSS under different strain amplitudes.

Under low strain amplitudes, the dislocation structure in ferrite of the unaged material is dominated by dislocation lines. In contrast, the dislocation density in the aged material is extremely low, and the mottled structure caused by spinodal decomposition can be observed. This indicated that a very low degree of plastic deformation occurs in ferrite of the aged material under low strain amplitudes. When the strain amplitude increased to 0.6%, the dislocation structures in the ferrite phase of the unaged and aged materials changed significantly. The dislocation density in ferrite of the unaged material was much higher than that under low strain amplitude. The vein dislocation structures formed in ferrite of the aged material under high strain amplitude, indicating that the ferrite phase underwent severe plastic deformation.

The high resolution transmission electron microscopy (HRTEM) image of ferrite in the fatigued aged specimen under 0.6% strain amplitude showed the lattice distortion (Figure 5e), which is similar to the deformed microstructures of the aged CDSS after tensile deformation reported in our previous investigation [25]. Figure 5f shows the corresponding orientation distribution of the HRTEM image, indicating that ferrite in the aged CDSS was divided into nanoscale regions with different orientations after deformation. These regions have a similar dimension as the Cr-enriched and Cr-depleted domains in ferrite induced by spinodal decomposition during thermal aging.

After thermal aging, the ferritic phase spinodally decomposed into Cr-enriched and Cr-depleted domains, which caused hardening and embrittlement in the ferrite. Severe plastic deformation in ferrite of the aged CDSS during cyclic loading under high strain amplitude caused the cleavage cracking in the hardened ferrite phases. The premature failure of ferrite in the aged CDSS accelerated the propagation of fatigue crack and thus shortens the LCF life.

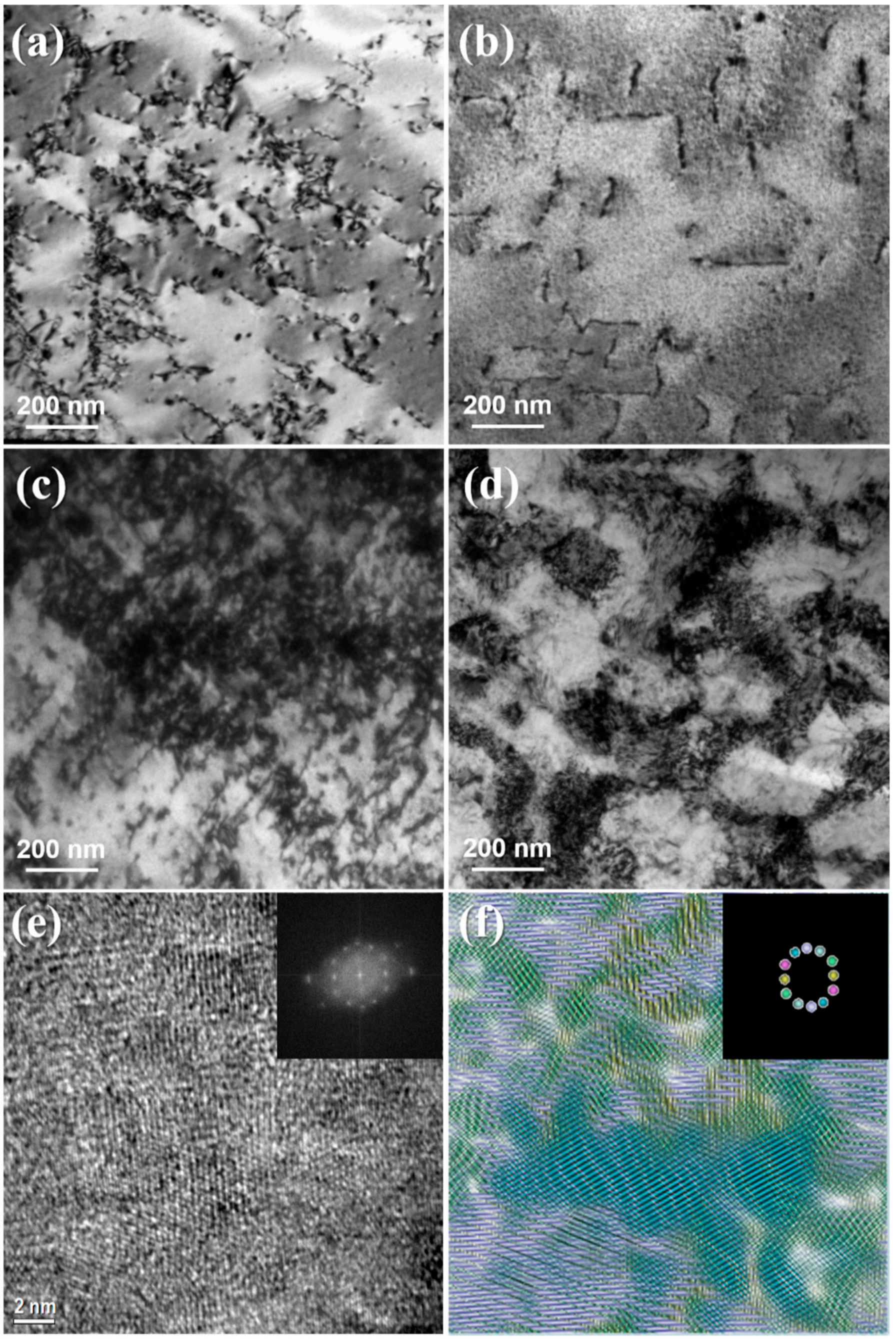

Figure 5. (**a**–**d**) Transmission electron microscopy (TEM) images of ferrite in the fatigued specimen of the unaged (**a**,**c**) and aged (**b**,**d**) under strain amplitude of 0.3% (**a**,**b**) and 0.6% (**c**,**d**). (**e**) High resolution TEM image of ferrite in the fatigued specimen aged at 400 °C for 10,000 h. (**f**) The corresponding orientation distribution of (**e**).

4. Conclusions

In this study, the effects of thermal aging on the low cycle fatigue behaviors of cast duplex stainless steels were investigated. The effect of thermal aging on the fatigue life was closely related to the strain amplitude: An increase with increasing aging time at low strain amplitudes while declining at high strain amplitude. The fatigue fracture morphologies of CDSS changed from fatigue fringes in both ferrite and austenite to fatigue fringes in austenite and cleavage cracks in ferrite. Under the cyclic loading of the high strain amplitude, severe plastic deformation in ferrite of the aged CDSS led to the cleavage cracking in the hardened ferrite phases, which accelerated the propagation of fatigue crack and shortened the fatigue life.

Author Contributions: X.W. and Y.W. designed the research project; S.L. performed the experiments, analyzed the data, and wrote the manuscript; all the authors contributed to the discussions and commented on the manuscript.

Funding: This work was financially supported by the National Natural Science Foundation of China (NSFC) (Grant No. 51601013) and the State Key Laboratory for Advanced Metals and Materials (Grant No. 2018Z-25).

Conflicts of Interest: The authors declare no conflict of interest.

References

1. Chung, H.M. Aging and life prediction of cast duplex stainless steel components. *Int. J. Pres. Ves. Pip.* **1992**, *50*, 179–213. [CrossRef]
2. Kawaguchi, S.; Sakamoto, N.; Takano, G.; Matsuda, F.; Kikuchi, Y.; Mráz, L. Microstructural changes and fracture behavior of CF8M duplex stainless steels after long-term aging. *Nucl. Eng. Des.* **1997**, *174*, 273–285. [CrossRef]
3. Yamada, T.; Okano, S.; Kuwano, H. Mechanical property and microstructural change by thermal aging of SCS14A cast duplex stainless steel. *J. Nucl. Mater.* **2006**, *350*, 47–55. [CrossRef]
4. Chung, H.M.; Leax, T.R. Embrittlement of laboratory and reactor aged CF3, CF8, and CF8M duplex stainless steels. *Mater. Sci. Tech.-Lond.* **1990**, *6*, 249–262. [CrossRef]
5. Timofeev, B.T.; Nikolaev, Y.K. About the prediction and assessment of thermal embrittlement of Cr–Ni austenitic–ferritic weld metal and castings at the ageing temperatures 260–425 °C. *Int. J. Pres. Ves. Pip.* **1999**, *76*, 849–856. [CrossRef]
6. Shiao, J.J.; Tsai, C.H.; Kai, J.J.; Huang, J.H. Aging embrittlement and lattice image analysis in a Fe-Cr-Ni duplex stainless steel aged at 400 °C. *J. Nucl. Mater.* **1994**, *217*, 269–278. [CrossRef]
7. Chandra, K.; Kain, V.; Bhutani, V.; Raja, V.S.; Tewari, R.; Dey, G.K.; Chakravartty, J.K. Low temperature thermal aging of austenitic stainless steel welds: Kinetics and effects on mechanical properties. *Mater. Sci. Eng. A* **2012**, *534*, 163–175. [CrossRef]
8. Pareige, C.; Novy, S.; Saillet, S.; Pareige, P. Study of phase transformation and mechanical properties evolution of duplex stainless steels after long term thermal ageing (>20 years). *J. Nucl. Mater.* **2011**, *411*, 90–96. [CrossRef]
9. Zhang, B.; Xue, F.; Li, S.L.; Wang, X.T.; Liang, N.N.; Zhao, Y.H.; Sha, G. Non-uniform phase separation in ferrite of a duplex stainless steel. *Acta Mater.* **2017**, *140*, 388–397. [CrossRef]
10. Brown, J.E.; Cerezo, A.; Godfrey, T.J.; Hetherington, M.G.; Smith, G.D.W. Quantitative atom probe analysis of spinodal reaction in ferrite phase of duplex stainless steel. *Mater. Sci. Tech.* **1990**, *6*, 293–300. [CrossRef]
11. Soriano-Vargas, O.; Avila-Davila, E.O.; Lopez-Hirata, V.M.; Cayetano-Castro, N.; Gonzalez-Velazquez, J.L. Effect of spinodal decomposition on the mechanical behavior of Fe–Cr alloys. *Mater. Sci. Eng. A* **2010**, *527*, 2910–2914. [CrossRef]
12. Danoix, F.; Auger, P. Atom probe studies of the Fe-Cr system and stainless steels aged at intermediate temperature: A review. *Mater. Charact.* **2000**, *44*, 177–201. [CrossRef]
13. Pumphrey, P.H.; Akhurst, K.N. Aging kinetics of CF3 cast stainless steel in temperature range 300–400 °C. *Mater. Sci. Tech.-Lond.* **1990**, *6*, 211–220. [CrossRef]
14. Bonnet, S.; Bourgoin, J.; Champredonde, J.; Guttmann, D.; Guttmann, M. Relationship between evolution of mechanical properties of various cast duplex stainless steels and metallurgical and aging parameters: Outline of current EDF programmes. *Mater. Sci. Tech.-Lond.* **1990**, *6*, 221–229. [CrossRef]
15. Hale, G.E.; Garwood, S.J. Effect of aging on fracture behaviour of cast stainless steel and weldments. *Mater. Sci. Tech.-Lond.* **1990**, *6*, 230–236. [CrossRef]
16. Tavares, S.A.C.S. Tensile properties of duplex UNS S32205 and lean duplex UNS S32304 steels and the influence of duration 475 °C aging. *Mater. Res.* **2012**, *15*, 859–864. [CrossRef]
17. Li, S.L.; Wang, Y.L.; Zhang, H.L.; Li, S.X.; Zheng, K.; Xue, F.; Wang, X.T. Microstructure evolution and impact fracture behaviors of Z3CN20-09M stainless steels after long-term thermal aging. *J. Nucl. Mater.* **2013**, *433*, 41–49. [CrossRef]

18. Li, S.L.; Zhang, H.L.; Wang, Y.L.; Li, S.X.; Zheng, K.; Xue, F.; Wang, X.T. Annealing induced recovery of long-term thermal aging embrittlement in a duplex stainless steel. *Mater. Sci. Eng. A* **2013**, *564*, 85–91. [CrossRef]
19. Chandra, K.; Singhal, R.; Kain, V.; Raja, V.S. Low temperature embrittlement of duplex stainless steel: Correlation between mechanical and electrochemical behavior. *Mater. Sci. Eng. A* **2010**, *527*, 3904–3912. [CrossRef]
20. Li, S.; Wang, Y.; Li, S.; Zhang, H.; Xue, F.; Wang, X. Microstructures and mechanical properties of cast austenite stainless steels after long-term thermal aging at low temperature. *Mater. Design* **2013**, *50*, 886–892. [CrossRef]
21. Chen, W.; Xue, F.; Tian, Y.; Yu, D.; Yu, W.; Chen, X. Effect of thermal aging on the low cycle fatigue behavior of Z3CN20.09M cast duplex stainless steel. *Mater. Sci. Eng. A* **2015**, *646*, 263–271. [CrossRef]
22. Llanes, L.; Mateo, A.; Iturgoyen, L.; Anglada, M. Aging effects on the cyclic deformation mechanisms of a duplex stainless steel. *Acta Mater.* **1996**, *44*, 3967–3978. [CrossRef]
23. Sahu, J.K.; Krupp, U.; Christ, H.J. Fatigue crack initiation behavior in embrittled austenitic–ferritic stainless steel. *Int. J. Fatigue* **2012**, *45*, 8–14. [CrossRef]
24. Marrow, T.J.; King, J.E. Fatigue crack propagation mechanisms in a thermally aged duplex stainless steel. *Mater. Sci. Eng. A* **1994**, *183*, 91–101. [CrossRef]
25. Li, S.; Wang, Y.; Wang, X. In situ observation of the deformation and fracture behaviors of Long-Term thermally aged cast duplex stainless steels. *Metals* **2019**, *9*, 258. [CrossRef]